



Effect of RF sputtering power and vacuum annealing on the properties of AZO thin films prepared from ceramic target in confocal configuration

Fatiha Challali, Djelloul Mendil, Tahar Touam, Thierry Chauveau, Valérie Bockelée, Alexis Garcia Sanchez, Azeddine Chelouche, Marie-Paule Besland

► To cite this version:

Fatiha Challali, Djelloul Mendil, Tahar Touam, Thierry Chauveau, Valérie Bockelée, et al.. Effect of RF sputtering power and vacuum annealing on the properties of AZO thin films prepared from ceramic target in confocal configuration. *Materials Science in Semiconductor Processing*, 2020, 118, pp.105217. <10.1016/j.mssp.2020.105217>. <hal-03011753>

HAL Id: hal-03011753

<https://hal.science/hal-03011753v1>

Submitted on 27 Nov 2020

HAL is a multi-disciplinary open access archive for the deposit and dissemination of scientific research documents, whether they are published or not. The documents may come from teaching and research institutions in France or abroad, or from public or private research centers.

L'archive ouverte pluridisciplinaire **HAL**, est destinée au dépôt et à la diffusion de documents scientifiques de niveau recherche, publiés ou non, émanant des établissements d'enseignement et de recherche français ou étrangers, des laboratoires publics ou privés.



HAL Authorization

Effect of RF sputtering power and vacuum annealing on the properties of AZO thin films prepared from ceramic target in confocal configuration

Fatiha Challali^{a,*}, Djelloul Mendil^{b,c}, Tahar Touam^{b,c}, Thierry Chauveau^a, Valérie Bockelée^a, Alexis Garcia Sanchez^a, Azeddine Chelouche^d, Marie-Paule Besland^e

^a Laboratoire des Sciences des Procédés et des Matériaux, UPR CNRS 3407, Université Sorbonne Paris Nord, France

^b Laboratoire des Semi-conducteurs, Université Badji Mokhtar-Annaba, 23000 Annaba, Algeria

^c Unité de Recherche en Optique et Photonique Centre de Développement des Technologies Avancées, Université de Sétif 1 campus El-Bez, 19000 Sétif, Algeria

^d Laboratoire de Génie de l'Environnement, Université de Bejaia, 06000 Bejaia, Algeria

^e Université de Nantes, CNRS, Institut des Matériaux Jean Rouxel, IMN, F-44000 Nantes, France

* Corresponding author: fatiha.challali@univ-paris13.fr

Abstract

Aluminum-doped zinc oxide (AZO) thin films are deposited on glass substrate by radio frequency (RF) magnetron sputtering method in confocal configuration at room temperature (RT). Several techniques are used to investigate the effects of sputtering power, from 50 to 300 W, on structural, optical and electrical properties. It is found, from Grazing Incidence X-Ray Diffraction (GIXRD) analysis, that the sputtering power has a great influence on the crystalline quality of AZO films. A preferential orientation along the c-axis is obtained at lower sputtering power of 50 W. XPS analysis confirms the existence of only Zn and Al in the oxidized state in accordance with the XRD results. SEM and AFM observations of AZO films reveal dense and homogenous distribution of small grains on the surface. Analysis by UV-Vis-NIR spectroscopy at RT reveals that the average optical transmittance in the visible range (400-800 nm) of the AZO thin films is higher than 75%. Hall-effect measurements put into evidence that the electrical resistivity of the films increases with the increase of the sputtering power. A low resistivity of $1.65 \times 10^{-3} \Omega \cdot \text{cm}$ is obtained for the lowest sputtering power (50W). Moreover, AZO thin film deposited at 50 W and annealed for 1h at 400°C under vacuum shows a lower resistivity of $5.75 \times 10^{-4} \Omega \cdot \text{cm}$, an average optical transmission above 86% and a high figure of merit (Φ_{TC}) value of $3.4 \times 10^{-3} \Omega^{-1} \text{sq}$ which suggests that

the fabricated AZO thin films are promising for optoelectronic devices in the UV region.

Keywords: Zinc oxide; AZO thin films; RF sputtering power; vacuum annealing; optoelectronics properties.

1. Introduction

In recent years, Zinc oxide (ZnO) has emerged as a potential transparent conductive oxide (TCO) candidate due to its unique and remarkable properties, including a good transparency over visible and near infrared light range, wide band gap of more than 3.3 eV and a good conductivity as n-type semiconductor thanks to a high carrier density. Furthermore, non-toxicity, high chemical stability as well as abundant availability of zinc has enabled its choice as a lower cost alternative for TCO's applications [1–3]. In addition, ZnO thin films doped with Al, Ga or In demonstrate high optical transmittance and low electrical resistivity for optoelectronic device applications. Particularly, Aluminum-doped Zinc oxide (AZO) thin films have shown the lowest resistivity among doped ZnO thin films [4, 5].

Various deposition methods have been used for the growth of AZO thin films including electrochemical deposition [6], Chemical vapor deposition (CVD) [7], pulsed laser ablation [8], sol-gel method [9], spray pyrolysis [10] and magnetron sputtering [11]. On the one hand, CVD techniques allow a large scale production with two major drawbacks: high process temperature and high costs. On the other hand, Sol-gel and spray pyrolysis are simple techniques with the advantages of low cost and low process temperature. Nevertheless, the obtained films exhibit lower quality with resistivity 5 times higher than those elaborated by other methods. Pulsed laser deposition (PLD) and magnetron sputtering are involved under vacuum and need high equipment investment. However, PLD produces excellent stoichiometric films with few structural defects, but deposition rates are low and scale up to industrial production has not been reached yet. On the

contrary, Magnetron Sputtering (MS) is one of the most extensively used techniques for TCO and AZO films deposition in particular. Indeed, this deposition technique has several advantages, such as low processing temperature, good film's adhesion, good thickness uniformity, high density of the films and well established up scaling to large areas. In addition, the process parameters such as working pressure, substrate temperature, sputtering power, are easy to control.

The sputtering power is one of the first order process parameters. Published works shown that, electrical and optical properties of the AZO films are dependent on their structural and morphological characteristics. Films properties are largely depend on the growth process during magnetron sputtering and easily controlled by the sputtering power. Moreover, the annealing in inert atmosphere is considered as an efficient parameter to improve crystalline quality and cure intrinsic defects, leading thus to improvement of both electrical and optical properties of the AZO thin films without modification of chemical composition. However, the annealing temperature of AZO films might be limited regarding the applications. Generally, annealing temperature should be lower than 500°C and appropriate to the substrate nature, i.e. semiconductor or glass substrates.

In this study, AZO thin films were successfully deposited on large area glass substrate at room temperature using RF magnetron sputtering in confocal configuration. We focus on the effect of sputtering power and annealing temperature on the structural, optical, morphological and electrical properties and, finally, we highlight the best experimental conditions to reach deposited films with electrical and optical properties both optimized.

2. Experimental details

2.1. Sample preparation

AZO thin films were deposited by RF magnetron sputtering on borosilicate glass substrates at room temperature from a 2-inch diameter commercial ZnO:Al₂O₃ (98:2wt.%) ceramic target with 99.99% purity in confocal configuration. **Indeed, in conventional top down sputtering, the target diameter should be larger than the substrate to achieve acceptable film uniformity. Confocal sputtering involves positioning of the target at 67° with respect to the substrate vertical axis** as shown in Fig. 1. The target-to-substrate distance was held as 120 mm. To improve the uniformity of the deposited films, the substrate holder was rotated axially at 10 rpm. The glass substrates were ultrasonically cleaned using acetone, methanol, and deionized water, and then dried in blowing nitrogen. The chamber was initially evacuated to a base pressure under 2×10^{-5} Pa. During deposition, working pressure was fixed at 0.5 Pa using a VAT valve controller and pure argon (Ar) as working gas with a fixed flow rate of 20 sccm (standard cubic centimeters per minute). The sputtering power applied to the target was varied in the range of 50-300W. The films thickness in the range of 115 to 180 nm was obtained by adjusting deposition time. Prior to the film deposition, pre-sputtering step was performed for 5 min at 300 W in a 40 sccm Ar gas flow to remove any contamination from the target surface and ensure a reproducible target surface state before each deposition. Besides, to consider the effect of the annealing temperature on AZO thin films properties, the films deposited using the optimized power were subsequently annealed under vacuum for 1 hour at 200 and 400°C. The base pressure of the chamber during vacuum annealing was kept at 10 Pa with Ar flow rate of 40 sccm.

2.2. Sample characterization

The crystalline structure of AZO films was investigated by GIXRD, using a Thermo Fisher Inel Equinox 1000 diffractometer with Cu-K α_1 radiation ($\lambda=1.54056\text{\AA}$) in $\omega/2\theta$ mode. The incidence angle was set to 2° and kept constant during acquisition (curved sensitive position detection with 2θ in the range of 0°-115°). The surface morphology

and cross-section of the films were observed using a high-resolution ZEISS Supra 40VP FEG Scanning Electron Microscope (SEM). The film thickness was determined using cross-sectional SEM micrographs. The topography and surface roughness of the films were evaluated by Atomic Force Microscopy (AFM). The experiment was performed in contact mode by a Nanosurf Flex-AFM system equipped with a 10×10 μm high-resolution scanner. Image processing and root mean square roughness (R_{rms}) estimations were achieved by the Gwyddion software [12]. The chemical bonding states of zinc, aluminum and oxygen in AZO films were investigated using X-ray Photoelectron Spectroscopy (XPS). The analyses were performed over an area of 700×400 μm² on a Kratos Nova photoelectron spectrometer using a monochromatic Al-Kα X-Ray source (1486.6 eV) operating at 150 W. The pressure in the analysis chamber was kept below 10⁻⁸ Pa. All high-resolution Core level spectra have been analyzed and fitted using Casa XPS software [13]. Energy Dispersive X-ray Spectroscopy (EDS) analysis was also involved to detect the elemental composition of the AZO thin films deposited on silicon substrate with 5800-LV SEM at 10kV. The resistivity, Hall mobility and carrier concentration of the samples were measured by Hall-effect measurements under Van-der Pauw geometry using Ecopia HMS-5000 system at an applied magnetic field of 0.55 T. Optical transmission spectra were recorded using a safas UVmc² UV-Vis-NIR spectrophotometer in the wavelength range of 200-1100 nm. The optical bandgap energy was then extracted from the transmittance data. All these measurements were performed at RT.

3. Results and discussions

3.1. Structural properties

Fig. 2(a) shows the GIXRD patterns of AZO thin films grown on glass substrates at different RF sputtering powers (50 W, 100 W, 200 W and 300 W). As displayed, all AZO films are crystallized. All recorded diffraction peaks can be indexed in the *P63mc*

space group and are significant for hexagonal wurtzite structure. No peaks corresponding to metallic Zn, Al or other aluminum compound are detected in the GIXRD patterns. The diffraction peaks corresponding to (100), (002), (101), (102), (110), (103) and (112) crystallographic planes exhibit variables intensities with the sputtering power. To get further insights on the sputtering power effect, patterns have been refined using MAUD [14] software with Rietveld method to extract microstructural parameters as intensity ratio, crystallite size and lattice parameters. Rietveld refinements of GIXRD spectra are carried out using starting parameters from the zincite structural model (ICDD PDF# 04-016-6648). The obtained results are gathered in **Table 1** (reference values in last line). The intensity ratio I_{002}/I_{103} decreases gradually from 4.42 to 1.10 for the films deposited with power varying from 50 W to 300 W respectively. For the lowest sputtering power of 50 W, the pattern shows a very intense peak at 33.91° corresponding to (002) plane diffraction whereas all other detected peaks exhibit low intensities. The I_{002}/I_{103} ratio of 4.42 is three times greater than the reference ratio of 1.52, indicating that the film is preferentially oriented along the c-axis; this preferential growth plane is due to its low surface free energy. When the sputtering power increases from 100 to 300 W, the (002) Bragg peak decreases gradually, while the intensity of the neighboring peaks corresponding to (101) and (103) diffraction planes are significantly enhanced. For the highest power of 300 W, the ratio I_{002}/I_{103} of 1.1 is lower than the reference's one (1.52) indicating that the (103) peak becomes the most intense. This result provides evidence for a change in preferential orientation with the sputtering power. Furthermore, with increasing sputtering power, all diffraction peaks are shifted towards a lower diffraction angle. As an example, only the 2θ of the (002) diffraction peak is presented in **Table 1**. The peak shifts towards a smaller angle from 33.91° to 33.74° for the films deposited at 50 W to 300 W respectively, compared to the standard value of the diffraction peak of the ZnO

(34.41°). The diffraction peak shift might be related to compressive stresses within the bulk of deposited films. As displayed in [Table 1](#), an increase of lattice d-spacing from the 0.2629 to 0.2639 nm occurs when the sputtering power increase from 50 to 300 W as compared to the d-spacing of 0.2604 nm from the ZnO reference. The origin of the compressive stress can be attributed to lattice distortions in the AZO films due to the bombardment of sputtered species which increase with increasing sputtering power. The presence of compressive stresses has been previously reported for intrinsic and doped ZnO films deposited by RF magnetron sputtering by K.H. Ri et al [15]. The calculated average crystallite size is found to be 29.28, 15.65, 10.1 and 15.89 nm for the AZO samples grown at 50, 100, 200 and 300 W, respectively. Variations of the GIXRD patterns with the sputtering power reveals that power leads to crystallographic structure degradation and multi-preferred orientations growth, which may be attributed to the stress induced in the deposited films by the increasing sputtering power and the changes of energies required for AZO growth along the (002) versus other orientations. Thus, when the sputtering power is increased, the energy of the sputtered species is enhanced, promoting thus AZO growth along the (103) orientation which requires a larger surface energy. It can be concluded that AZO film deposited at lower sputtering power (50 W) has the best crystalline structure quality considering the extracted microstructure parameters. Malinowska et al. [16] have demonstrated that when the power is too high in RF sputtering process, the plasma species bombard the film surface with relatively high energy. This leads to the generation of surface defects and deterioration of film crystallinity. Our results are therefor in good agreement with their work.

3.2. Surface morphology

Top-view SEM micrographs and the corresponding cross-section (inset) of AZO thin films deposited at various RF power are shown in [Fig. 3\(a-d\)](#). It can be observed that the AZO films exhibit dense and homogenous distribution of small grains on the surface.

The surface morphology appears to be dependent on the RF power. The surface of the films deposited at 50, 100 and 200 W shows regular and rounded grains, whereas the film prepared with a high power of 300 W exhibits relatively elongated surface grains. The difference in the grains shape can be related to the mixed (002) and (103) crystalline preferential orientations as shown by GIXRD patterns. The corresponding SEM cross-section images (Insets of Fig. 3(a-d)) illustrate the evolution in crystallinity of the bulk AZO films as a function of sputtering power. It can be clearly seen that the growth mode of AZO films changes gradually from columnar to granular structure as the sputtering power is increasing, indicating that the growth mode and microstructure of AZO films are influenced by the RF power. The AZO film deposited at 50 W presents a columnar morphology along the vertical c-axis with circular-like crests. It is observed that the majority of the grains grew nearly perpendicular to the substrate, which is again in accordance with the XRD results. In contrast, from 100 to 200 W, the growth changes gradually towards a mixture of fine columns and small grains. At 300 W, the growth of the film changes and the cross-section view exhibits granular structures with different sizes.

Fig. 4(a-d) displays the two-dimensional (2D) AFM topography images of the AZO thin films deposited at different powers recorded over a $2.0\ \mu\text{m} \times 2.0\ \mu\text{m}$ scanning area. As can be observed from the AFM images, the AZO films exhibited smooth surface and regular grain morphology in agreement with SEM observations. The R_{rms} is estimated about 1.57, 2, 2.69 and 3.5 nm for the film deposited at 50, 100, 200 and 300 W respectively. This trend in R_{rms} could be attributed to the increase in the bombardment of the surface by the sputtered species at high power.

3.3. XPS analysis

Surface chemical composition and chemical state changes in the AZO thin films were analyzed by XPS. Survey scan spectra (not shown here) were collected in the -5 to 1200

eV range (binding energy). Fig.5 displays XPS core level spectra and the elemental components for (a) Zn 2p, (b) Al 2p and (c) O 1s for the AZO thin films grown at the four sputtering power values. They are calibrated in energy by setting carbon C 1s at 284.7 eV and fitted using a Shirley type base-line for the background and a pseudo-Voigt function for each component. The core level line of Zn 2p and Al 2p (Fig. 5 (a) and (b)) reveal high symmetry for all the AZO films. The Zn 2p_{3/2}, Zn2p_{1/2} and Al 2p core lines are centered at 1022.2±0.1 eV, 1045.2 eV and 74.6±0.1 eV, respectively. No signal is observed at binding energies of 1021.5 eV and 72.7 eV [17], respectively, which is a significant evidence for no metallic Zn or Al state. We can conclude that Zn and Al are only in the oxidized state. As can be seen in Fig.5 (c) for all analyzed AZO films, the O 1s core level signal can be decomposed in two components located at 530.3± 0.1 eV and 531.9±0.1 eV, respectively. In addition, a FWHM of 1.68 eV allows the fitting with only two components. Thus, the O 1s fitting does not need to introduce a third component as reported by some authors [18-19]. The attribution of the two components has been done thanks to the comparison of the O 1s core level recorded before and after a 60 s etching. The corresponding O 1s high resolution spectra recorded for the AZO sample deposited at 50 W before and after etching (Fig. 5(d)) clearly show a significant variation of the two components contributions. The relative intensity of the O_{II} contribution is largely decreased after etching from 32% to 6% meaning that this contribution is located at the very surface of the film. Conversely, the O_I component is enhanced from 24 to 42% after erosion step, since the signal is no more attenuated by surface contamination. Consequently, we can conclude that the O_{II} component at higher binding energy (531.9±0.1 eV) can be attributed to the presence of adsorbed oxygen species such as CO₂ and adsorbed H₂O or O₂, at the surfaces of the AZO films. The O_I component at lower binding energy (530.3± 0.1 eV) is related to the O-Zn bonds within the ZnO wurtzite structure, i.e. O atoms fully surrounded by Zn²⁺ cations or

substitutional Al^{3+} cations. Such results are in agreement with those reported by Correia et al. [20].

The chemical composition was estimated by XPS from the measured peak area using the relative sensitivity factors of Zn 2p, Al 2p and O 1s core levels, and taking into account only the O_1 area for the oxygen content. The aluminum content is close to 2% for all AZO films, i.e. close to the target Al content 2%. Moreover, according to EDS measurements, the atomic concentration of Al in all the AZO samples remains unchanged at 1.90 ± 0.1 at% regardless the sputtering power. The XPS results and EDS measurements are thus in excellent agreement.

3.4. Optical properties

To investigate the influence of RF power on the optical properties of AZO thin films, the optical transmittance of the films deposited at various sputtering power was measured with respect to air by UV-Vis-NIR spectrophotometer in the 200 to 1100 nm wavelength range. The results are plotted in Fig. 6(a). All AZO films show an average transmittance of 75-81% in the visible range (400-800 nm). This means that the sputtering power has a moderate effect on the transparency of the as-deposited thin films over the whole visible range. However, the short wavelength cut-off in transmittance spectra of AZO thin films has a clear shift towards higher wavelength values indicating a reduction of the optical band gap.

The direct optical band gap (E_g) of the AZO thin films was determined by using the technique based on the first derivative of transmittance (T), dT/dE , as a function of energy (E) [21]. Based on the transmittance spectra, Fig. 7(a) shows dT/dE as a function of E for the deposited AZO thin films versus RF power. Band gap values of 3.16, 3.25, 3.12 and 3.02 eV are obtained for the samples deposited at sputtering power of 50, 100, 200 and 300 W, respectively. It can be seen that the band gap decreases with increasing sputtering power. Similar trends of the optical band gap variation versus RF power have

also been reported in literature for sputtered AZO thin films. Sun et al. [22] have found that the optical band gap of AZO thin films deposited at RF power of 200, 300, 400 and 500 W were equal to 3.68, 3.62, 3.57 and 3.48 eV, respectively. They attributed such band gap value decrease to a carrier concentration decrease with increasing sputtering power. Patel and Rawal [23] reported a similar decrease from 3.29 eV to 3.22 eV of the optical band gap value for sputtered AZO thin films versus RF power variation from 60 W to 180 W respectively. However, It should be noted that the band gap of the AZO film prepared at 100 W is slightly blue-shifted due to the fact that its thickness is lower (115 nm) as compared to the average thickness of the other samples (167 nm) [24].

3.5. *Electrical properties*

Electrical properties of our sputtered AZO films have been obtained through Hall-effect measurements. Numerical data are given in [Table 2](#). The variations of electrical resistivity, carrier concentration and Hall mobility versus RF sputtering power are plotted in [Fig. 8\(a\)](#). It is clear that electrical properties of sputtered AZO thin films are dependent on deposition power in a very large extend. As the RF power increases from 50 to 300 W, the carrier density decreases from 21.1×10^{20} to $2.3 \times 10^{20} \text{ cm}^{-3}$, Hall mobility of free electrons decreases from 2.63 to 0.35 $\text{cm}^2/\text{V s}$ and the electrical resistivity increases from 1.65×10^{-3} to $75.8 \times 10^{-3} \text{ }\Omega\cdot\text{cm}$, i.e. more than a factor 45. Generally, in AZO thin films deposited at room temperature, the conduction is mainly influenced by the mobility. The decrease in carrier density and Hall mobility can be attributed to deterioration of thin film crystallinity, as evidenced previously by XRD analysis. The variations in grain size and film defects might be promoted by the increasing energy of the species occurring at high power. The best electrical properties for AZO films deposited at room temperature are obtained for those deposited at a low sputtering power of 50 W, with an electrical resistivity of $1.65 \times 10^{-3} \text{ }\Omega\cdot\text{cm}$. In this case, the Hall mobility and carrier density are, respectively, $2.63 \text{ cm}^2/\text{V.s}$ and $21.1 \times 10^{20} \text{ cm}^{-3}$:

those values are the best compromise in electrical properties. This result can be attributed to the best structural properties of deposited AZO film: a large preferential orientation along the c-axis, highest crystallite size (average size close to 30 nm), leading to a decrease of carrier diffusion at grain boundaries and interfaces and going along with an increase in the carrier lifetime.

To evaluate the quality and performance of the deposited AZO films, the figure of merit (Φ_{TC}) has been calculated for the deposited AZO thin films as defined by Haacke [25], using the following equation: $\Phi_{TC} = T^{10}/R_s$, where T is the transmittance (in this work we have used the average optical transmittance of the AZO films from 400 to 800 nm to evaluate the film's performances in the visible range) and R_s is the sheet resistance. Fig. 9 shows the plot of the Φ_{TC} for AZO thin films deposited with sputtering power in the range of 50-300W. We observe a decrease of the figure of merit when the sputtering power is increased from 50 to 300 W. As discussed above, the AZO thin films prepared using 50 W sputtering power exhibit better performances with simultaneously a low sheet resistance of 175 Ω/sq and an average transmittance of 75 % in the visible region. However, such values are not satisfying for films to be used as TCO. In order to improve the properties of the AZO film deposited at 50 W, two thin films deposited at the same time at room temperature have been subsequently annealed in vacuum for one hour at 200 and 400 °C, respectively. The results are presented and discussed in the following section.

3.6. Annealing effect on AZO films properties

From the XRD patterns shown in Fig. 2(b), the AZO thin films deposited at 50 W and annealed at 200 and 400 °C exhibit a (002) preferential orientation. The I_{002}/I_{103} diffraction peaks intensity ratio increases from 4.42 to 6.78 from the as-deposited sample and the annealed sample at 400°C, respectively. The average crystallite size increased after annealing from 29.28 nm for the as-deposited sample, to 38.12 nm for

the sample annealed at 400°C. Furthermore, the (002) plane diffraction peak shifts towards a higher angle from 33.91° to 34.06° for the as-deposited film and annealed film at 400°C respectively (Table 1). Thus, the initial compressive stress decreases after the annealing treatment. Also, the cell parameters decrease upon annealing and the final values are close to the reference's one. Such variation is significant for an improvement of crystalline quality of annealed films with annealing temperature. The SEM and AFM images (Fig. 3(b) and 4(b)) display films with denser surface and regular grain morphology when annealing temperature increased up to 400°C. The roughness of the annealed films increases from 1.75 to 3.03 nm (Table 2) which may be associated to the increased average crystallite size, as estimated from XRD data analysis. Fig. 6(b) shows transmittance spectra of the sputtered AZO thin films at 50 W associated with the conditions of as-deposited and annealed at 200 and 400°C, respectively. An average transmission of 75% in the visible range is obtained for the as-deposited film. After one hour annealing, the average transmittance is improved to 78% and 86% for the AZO films annealed at 200 and 400°C respectively. The optical transmittance is thus significantly improved by the annealing step. The variation of optical bandgap as a function of annealing temperature is extracted from the dT/dE plots gathered in Fig. 7(b). The band gap increases from 3.16 eV for as-deposited film to 3.27 eV and 3.33 eV for the films annealed at 200°C and 400°C, respectively. Such increase is attributed to the carrier density increase upon annealing resulting in the bandgap widening according to the Burstein-Moss model [26]. Fig. 8(b) shows the effect of an annealing step and the annealing temperature on the electrical properties of the AZO films deposited at 50W. The increase in both carrier concentration and Hall mobility leads, as expected to decrease resistivity, i.e. an increase in conductivity. The improvement in the electrical properties may be attributed to the reduction of grain boundaries of the AZO film with increasing the annealing temperature, resulting in an increase in the mobility of the

carriers. The factor of merit (Φ_{TC}) value of $3.4 \times 10^{-3} \Omega^{-1}\text{sq}$ after annealing at 400°C is 10 times higher than those calculated to the as-deposited films. It can be concluded that the film deposited at sputtering power of 50 W and annealed in vacuum for one hour at 400°C exhibits the best optical, electrical and structural properties. This result is a major issue for further applications of sputtered AZO films of this study as transparent conductive films.

4. Conclusions

AZO thin films have been successfully prepared on glass substrate by RF magnetron sputtering. The effects of sputtering power and annealing temperature on the electrical and optical properties have been discussed in this paper. XRD results have shown that AZO film deposited at a low power of 50 W has a larger average crystallite size in comparison with the films deposited at higher sputtering power. The obtained AZO film is preferentially oriented along the c-axis according to the intensity ratio of the diffraction peaks, which is attributed to a low surface free energy of the (002) plan. The data show that the crystallites in AZO films become smaller and the preferential orientation change gradually, as the sputtering power increases from 100 to 300 W. The variation of the XRD patterns with the sputtering power reveals that high sputtering power leads to structural degradation and multi-orientation growth. XPS analysis highlighted that, Zn and Al atoms existed only in their oxidized state in accordance with the XRD results, where no metallic phase was detected. SEM observations of AZO films have revealed dense and homogenous distribution of small grains on the surface. AFM results have demonstrated that the sputtering power does not significantly influence the surface roughness and grain size. The R_{rms} is found to increase from 1.57 to 3.5 nm when RF power is increased from 50 to 300 W. These trends could be attributed to the increase of the bombardment of the surface by the sputtered species at high power. All deposited AZO films exhibited average

transmittance of 75-81% in the visible range (400-800 nm). According to Hall Effect measurements, electrical properties of the AZO films are found to be largely modified by the RF deposition power. Hence, the carrier density and Hall mobility decrease, and therefore the electrical resistivity increases from 1.65×10^{-3} to $68.26 \times 10^{-3} \Omega \cdot \text{cm}$, with increasing sputtering power from 50 to 300 W, respectively. Optimized AZO films, with $5.75 \times 10^{-4} \Omega \cdot \text{cm}$ electrical resistivity, average visible transmission of 86% and high figure of merit (Φ_{TC}) value of $3.4 \times 10^{-3} \Omega^{-1} \text{sq}$, have been obtained at 50 W deposition power and after annealing at 400°C for 1h under vacuum. The present study shows that AZO thin films are potential and good candidates for optoelectronic devices in the UV region.

Acknowledgments

XPS and EDS analysis have been performed at Institut des Matériaux Jean Rouxel, Université de Nantes, France. The authors gratefully acknowledge Nicolas STEPHANT and Jonathan HAMON for EDS and XPS analysis respectively.

References

- [1] T. Minami, Transparent conducting oxide semiconductors for transparent electrodes, *Semicond. Sci. Technol.* 20 (2005) S35–S44. <https://doi.org/10.1088/0268-1242/20/4/004>.
- [2] R.A. Afre, N. Sharma, M. Sharon, Transparent conducting oxide films for various applications: A review, *Rev. Adv. Mater. Sci.* 53, 1 (2018) 79–89. <https://doi.org/10.1515/rams-2018-0006>.
- [3] K. Ellmer, Past achievements and future challenges in the development of optically transparent electrodes, *Nature Photon* 6 (2012) 809–817. <https://doi.org/10.1038/nphoton.2012.282>.
- [4] M. Asemi, M. Ahmadi, M. Ghanaatshoar, Preparation of highly conducting Al-doped ZnO target by vacuum heat treatment for thin film solar cell applications, *Ceram. Int.* 44 (2018) 12862–12868. <https://doi.org/10.1016/j.ceramint.2018.04.096>.
- [5] K. Ellmer, A. Klein, B. Rech, *Transparent Conductive Zinc Oxide Basics and Applications in Thin Film Solar Cells*, Springer, (2008).
- [6] A. Kumar, S. Valanarasu, V. Ganesh, M. Shkir, S. Al Faify, H. Algarni, Effect of potential voltages on key functional properties of transparent AZO thin films prepared

- by electrochemical deposition method for optoelectronic applications. *J. Mater. Sci.* 33, 11 (2018) 1523–1533. <https://doi.org/10.1557/jmr.2018.122>.
- [7] K.W. Johnson, S. Guruvenket R. A. Sailer, S. Phillip Ahrenkiel, D. L.Schulz Atmospheric pressure plasma enhanced chemical vapor deposition of zinc oxide and aluminum zinc oxide, *Thin Solid Films* 548 (2013) 210–219, <https://doi.org/10.1016/j.tsf.2013.09.060>.
- [8] X.Q. Gu, L.P. Zhu, L. Cao, Z.Z. Ye, H.P. He, P. Chu, Optical and electrical properties of ZnO:Al thin films synthesized by low-pressure pulsed laser deposition, *Mater. Sci. Semicond. Process.* 14 (2011) 48–51. <https://doi.org/10.1016/j.mssp.2011.01.003>.
- [9] K. D. Arun Kuma, S. Valanarasu, A. Kathalingam, V. Ganesh, M. Shkir, S. AlFaify, Effect of solvents on sol–gel spin-coated nanostructured Al-doped ZnO thin films: a film for key optoelectronic applications; *Applied Physics A* (2017) 123:801, <https://doi.org/10.1007/s00339-017-1426-z>.
- [10] M. Nasiri, S.M. Rozati, Muscovite mica as a flexible substrate for transparent conductive AZO thin films deposited by spray pyrolysis, *Mater. Sci. Semicond. Process.* July 2018 81:38-43, <https://doi.org/10.1016/j.mssp.2018.03.009>.
- [11] N. Hernandez-Como, A. Morales-Acevedo, M. Aleman, I. Mejia, M.A. Quevedo-Lopez, Al-doped ZnO thin films deposited by confocal sputtering as electrodes in ZnO-based thin-film transistors, *Microelectron. Eng.* 150 (2016) 26–31. <http://dx.doi.org/10.1016/j.mee.2015.10.017>.
- [12] D. Nečas, P. Klapetek, Gwyddion: open-source software for SPM data analysis, *Cent. Eur. J. Phys.* 10 (2012) 181–188. <https://doi.org/10.2478/s11534-011-0096-2>.
- [13] N. Fairley, <http://www.casaxps.com>, © Casa software Ltd. 2005.
- [14] L. Lutterotti, S. Matthies, H. Wenk, MAUD: a friendly Java program for material analysis using diffraction, *CPD Newsletter* 21 (1999) 14–15. <http://hdl.handle.net/11572/38076>
- [15] K.H. Ri, Y. Wang, W.L. Zhou, J.X. Gao, X.J. Wang, J. Yu, The structural properties of Al doped ZnO films depending on the thickness and their effect on the electrical properties, *Appl. Surf. Sci.* 258 (2011) 1283–1289. <https://doi.org/10.1016/j.apsusc.2011.07.022>.
- [16] D. Dimova-Malinovska, N.Tzenov, M.Tzolov, L.Vassilev, Optical and electrical properties of R.F. magnetron sputtered ZnO:Al thin films, *Mater. Sci. Eng. B* 52 (1998) 59. [https://doi.org/10.1016/S0921-5107\(97\)00210-9](https://doi.org/10.1016/S0921-5107(97)00210-9)

- [17] N. Srinatha, Y.S. No, V.B. Kamble, S. Chakravarty, N.S Murthy, B. Angadi, A. M. Umarji, W. K. Choi, Effect of RF power on the structural, optical and gas sensing properties of RF-sputtered Al doped ZnO thin films, *RSC Adv.* 6 (2016) 9779–9788. <https://doi.org/10.1039/C5RA22795J>.
- [18] D. K. Kim, H.B. Kim, Room temperature deposition of Al-doped ZnO thin films on glass by RF magnetron sputtering under different Ar gas pressure, *J. Alloys Compd.* 509 (2011) 421–425. <https://doi.org/10.1016/j.jallcom.2010.09.047>.
- [19] N. Kumar, A. Dubey, B. Bahrami, S. Venkatesan, Q. Qiao, M. Kumar, Origin of high carrier mobility and low residual stress in RF superimposed DC sputtered Al doped ZnO thin film for next generation flexible devices, *Appl. Surf. Sci.* 436 (2018) 477–485. <https://doi.org/10.1016/j.apsusc.2017.11.274>.
- [20] F.C. Correia, N. Bundaleski, O.M. Teodoro, M.R. Correia, L. Rebouta, A. Mendes, C.J. Tavares, XPS analysis of ZnO:Ga films deposited by magnetron sputtering: Substrate bias effect, *Appl. Surf. Sci.* 458 (2018) 1043–1049. <https://doi.org/10.1016/j.apsusc.2018.07.135>.
- [21] T. Touam, M. Atoui, I. Hadjoub, A. Chelouche, B. Boudine, A. Fischer, A. Boudrioua, A. Doghmane, Effects of dip-coating speed and annealing temperature on structural, morphological and optical properties of sol-gel nano-structured TiO₂ thin films, *Eur. Phys. J. Appl. Phys.* 67 (2014) 30302. <https://doi.org/10.1051/epjap/2014140228>.
- [22] Y.H. Sun, H.L. Wang, J. Chen, L. Fang, L. Wang, Structural and optoelectronic properties of AZO thin films prepared by RF magnetron sputtering at room temperature, *Trans. Nonferrous Met. Soc. China* 26 (2016) 1655–1662. [https://doi.org/10.1016/S1003-6326\(16\)64275-9](https://doi.org/10.1016/S1003-6326(16)64275-9).
- [23] K.H. Patel, S.K. Rawal, Influence of power and temperature on properties of sputtered AZO films, *Thin Solid Films* 620 (2016) 182–187. <https://doi.org/10.1016/j.tsf.2016.08.073>
- [24] K. Necib, T. Touam, A. Chelouche, L. Ouarez, D. Djouadi, B. Boudine, Investigation of the effects of thickness on physical properties of AZO sol-gel films for photonic device applications, *J. Alloys Compd.* 735 (2018) 2236–2246. <https://doi.org/10.1016/j.jallcom.2017.11.361>.
- [25] G. Haacke, New figure of merit for transparent conductors, *J. Appl. Phys.* 47 (1976) 4086–4089. <https://doi.org/10.1063/1.323240>

[26] T.S Moss, The interpretation of the properties of indium antimonide; Proceedings of the Physical Society. Section B, 67 10 (1954) 775. <https://doi.org/10.1088/0370-1301/67/10/306>.

Table captions

Table 1: Structural parameters extracted from XRD analysis of AZO films deposited at various sputtering powers and for films deposited at 50 W after annealing at 200 and 400°C for 1 h under vacuum conditions. The last line “ref. data” gives reference values from the zincite structural model (ICDD PDF# 04-016-6648).

Table 2: Roughness, resistivity, Hall mobility, carrier concentration, average transmittance, optical band gap and factor of merit (Φ_{TC}) for the as-deposited AZO thin films versus the sputtering power and for films deposited at 50 W after annealing at 200 and 400°C for 1 h under vacuum conditions.

Figures captions

Fig. 1. Schematic representation of the experimental setup.

Fig. 2. Grazing incidence XRD patterns of AZO thin films (a) deposited at different RF sputtering powers and (b) deposited at 50 W and annealed at 200 and 400°C for 1 h under vacuum conditions.

Fig. 3. Top-view SEM images of AZO thin films (a-d) deposited at various RF powers with the corresponding cross-section (inset) and (e-f) deposited at 50 W and annealed at 200 and 400°C.

Fig. 4. 2D AFM images of AZO thin films (a-d) deposited at different RF sputtering powers and (e-f) deposited at 50 W and annealed at 200 and 400°C.

Fig. 5. XPS core level spectra recorded for AZO thin films versus RF sputtering power (50, 100, 200, 300 W): (a) Zn 2p, (b) Al 2p, (c) O 1s and (d) O 1s core level for the as deposited AZO-50 W film and after 60 s soft etching.

Fig. 6. Optical transmittance spectra of AZO thin films (a) deposited at different RF sputtering powers and (b) deposited at 50 W and annealed at 200 and 400°C.

Fig. 7. dT/dE curves based on transmittance spectra of AZO thin films (a) deposited at different RF sputtering powers and (b) deposited at RF power of 50 W and annealed at 200 and 400°C.

Fig. 8. Variation of resistivity, carrier concentration and mobility of AZO thin films (a) with RF sputtering power and (b) as a function of annealing temperature of the films deposited at RF power of 50 W.

Fig. 9. Figure of merit of AZO thin films versus RF power in the 50-300 W range. The inset shows the effect of annealing temperature on the figure of merit of AZO thin films deposited at 50 W.

Table 1

Sputtering power (W)	Vacuum annealing (°C)	002 plane			Crystallite size (nm)				lattice parameters (nm)	
		2 θ (°)	d-spacing (nm)	I ₀₀₂ /I ₁₀₃	(002) plane	(101) plane	(103) plane	avg. size	a	c
50	-	33.91	0.2629	4.42	48.01	24.35	15.47	29.28	0.3267	0.5259
50	200	33.92	0.2631	3.98	47.92	23.96	16.21	29.35	0.3271	0.5262
50	400	34.06	0.2614	6.78	58.22	24.45	31.71	38.12	0.3260	0.5214
100	-	33.68	0.2635	2.80	14.56	20.96	11.44	15.65	0.3311	0.5271
200	-	33.53	0.2636	2.22	11.43	11.08	7.78	10.10	0.3312	0.5279
300	-	33.74	0.2639	1.10	24.54	13.79	9.21	15.85	0.3307	0.5274
Ref.	-	34.41	0.2604	1.52	-	-	-	-	0.3251	0.5208

Table 2

Sputtering power (W)	Vacuum annealing (°C)	R_{rms} (nm)	Resistivity ($10^{-3} \Omega \cdot cm$)	Hall mobility ($cm^2/V \cdot s$)	Carrier concentration ($10^{20} cm^{-3}$)	Average transmittance (%)	Optical gap (eV)	Φ_{TC} ($10^{-4} \Omega^{-1} sq$)
50	-	1.57	1.65	2.63	21.10	75	3.16	3.04
50	200	2.30	0.81	2.65	29.45	78	3.27	9.27
50	400	3.03	0.57	2.79	38.85	86	3.33	33.98
100	-	2	4.51	1.34	10.4	79	3.25	1.26
200	-	2.69	49.42	1.18	2.61	81	3.12	0.17
300	-	3.5	75.80	0.35	2.33	79	3.02	0.14

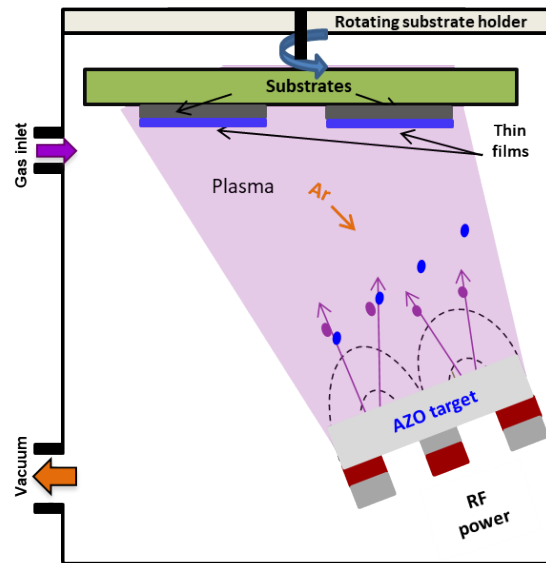


Fig. 1

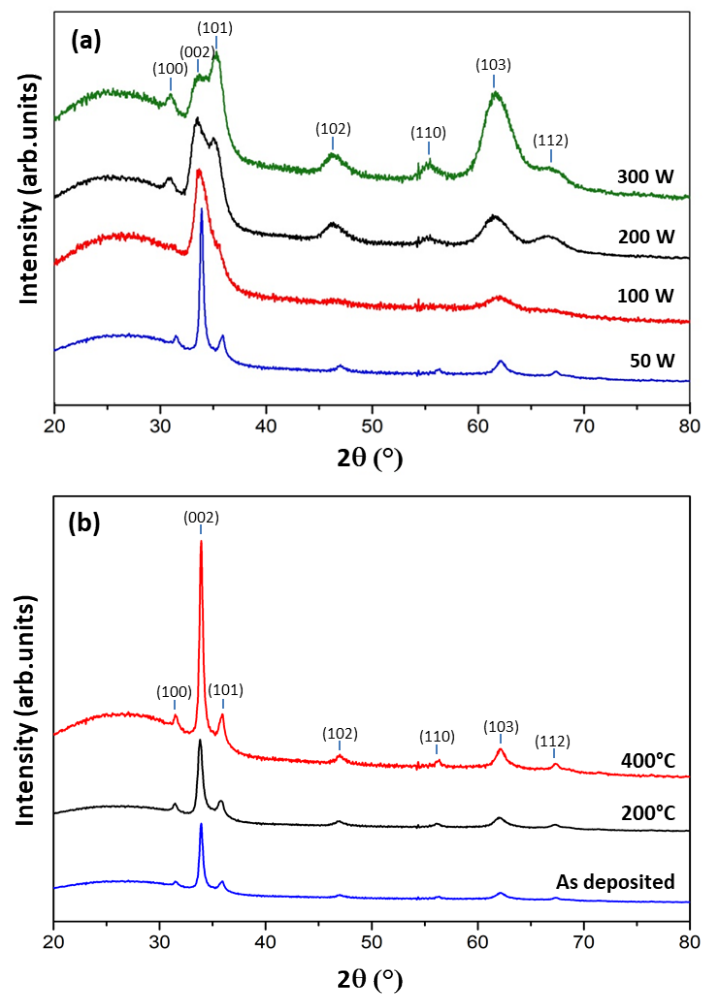


Fig. 2

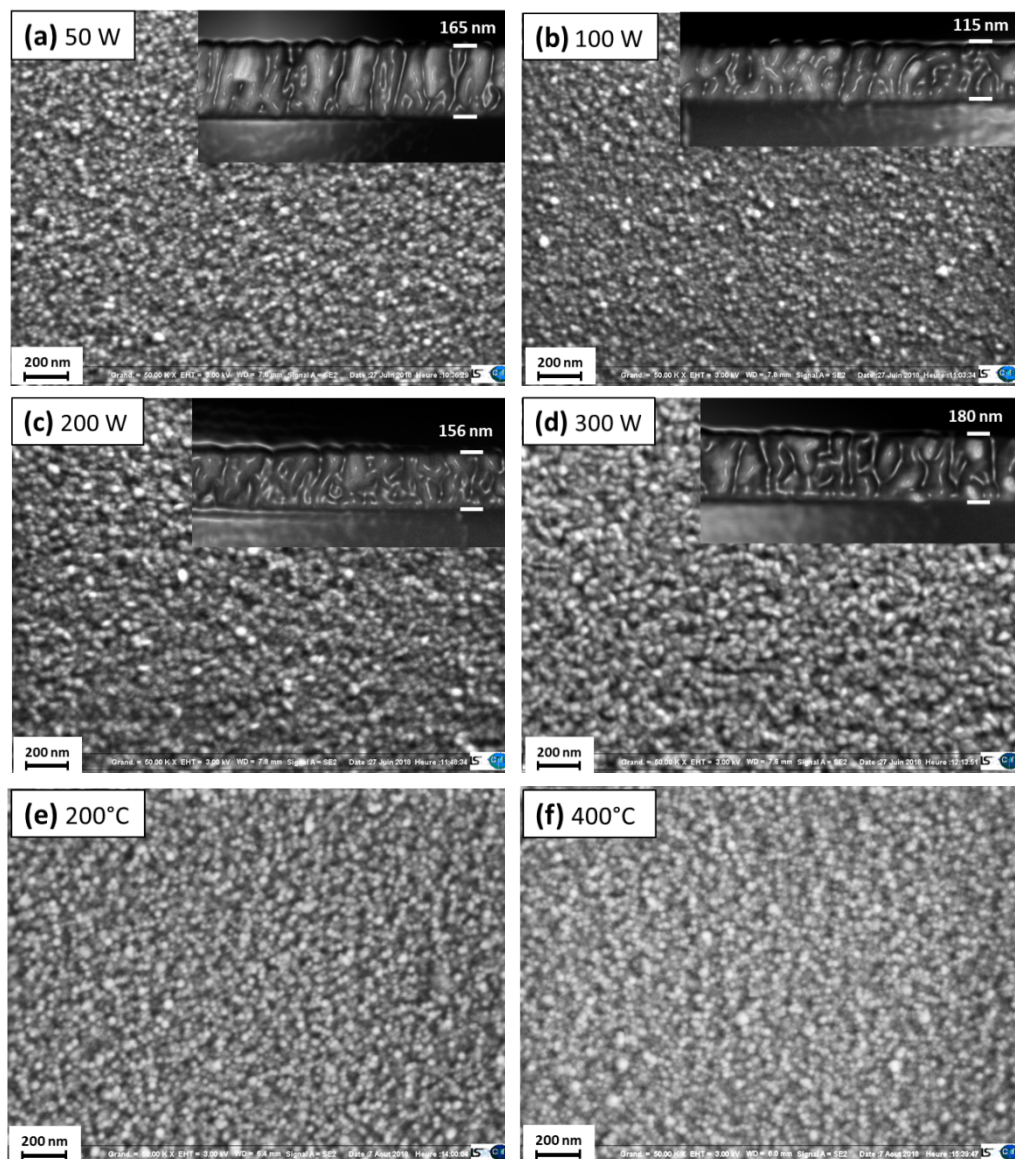


Fig. 3

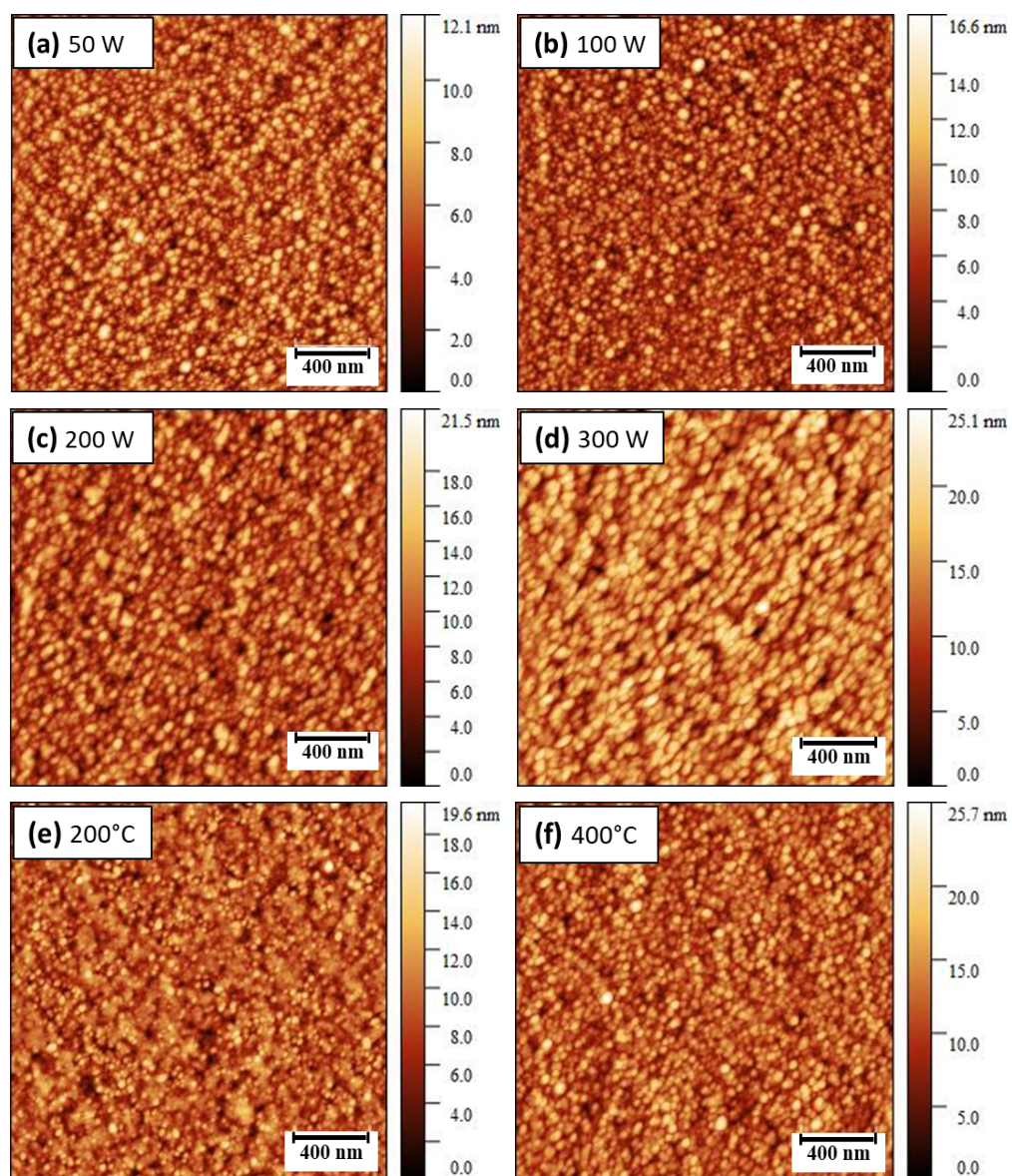


Fig. 4

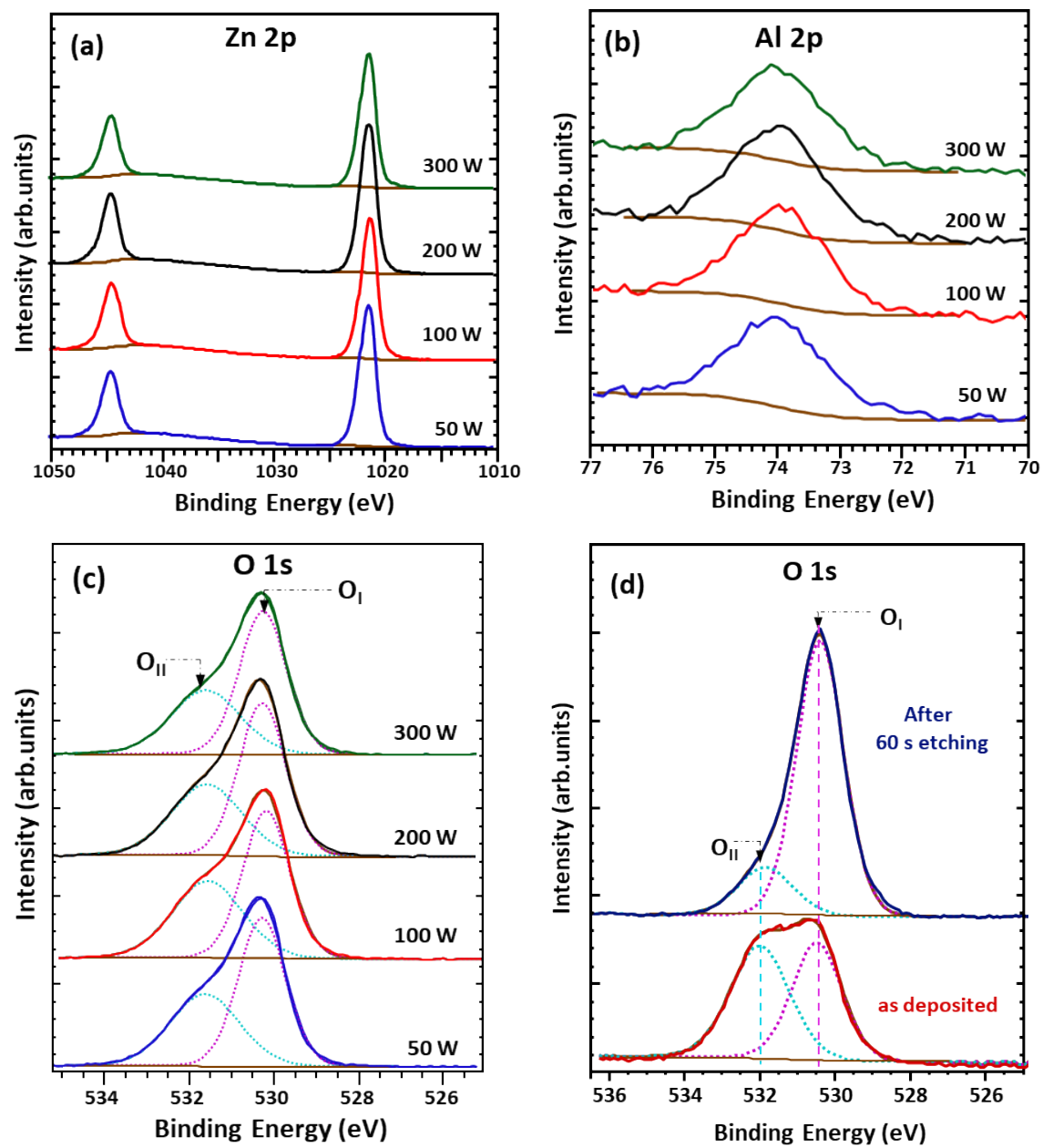


Fig. 5.

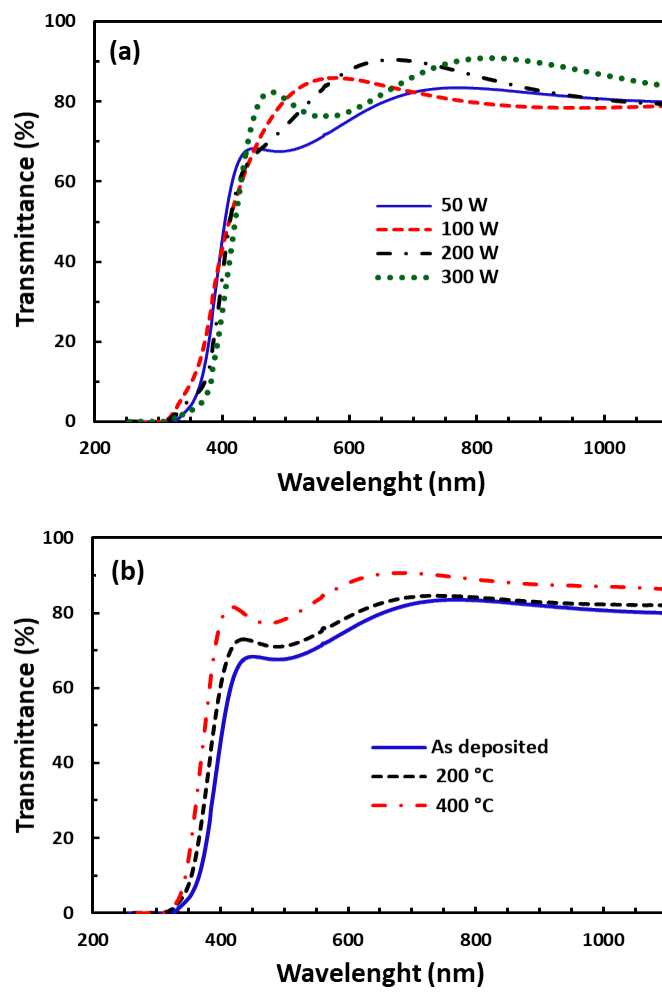


Fig. 6

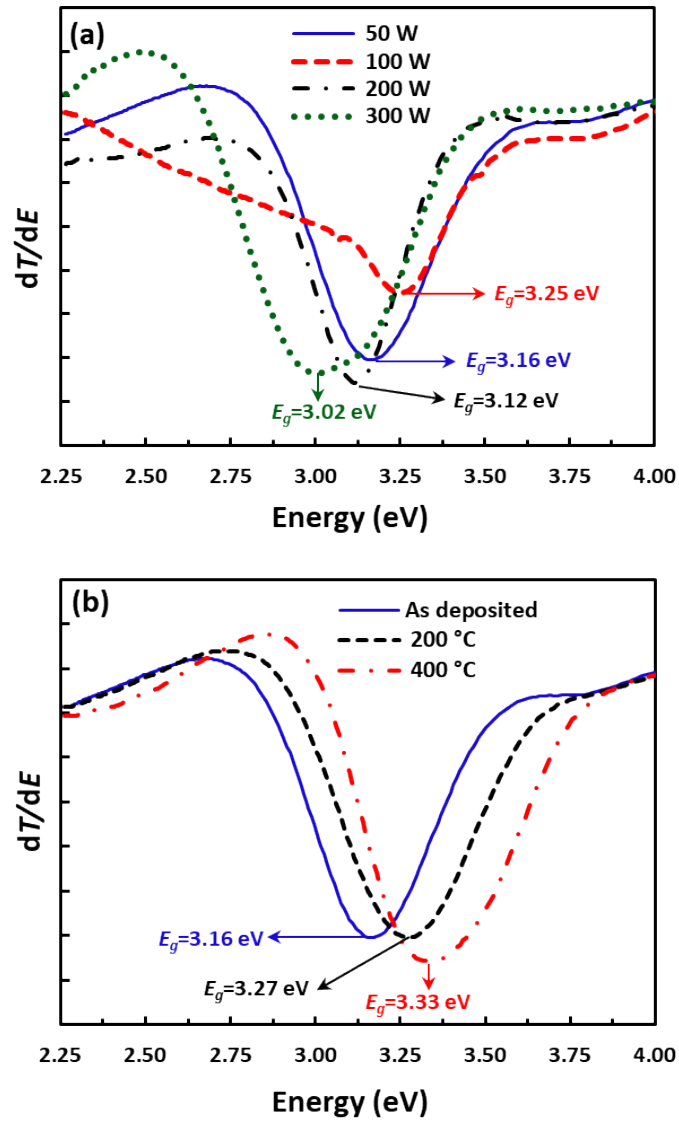


Fig. 7

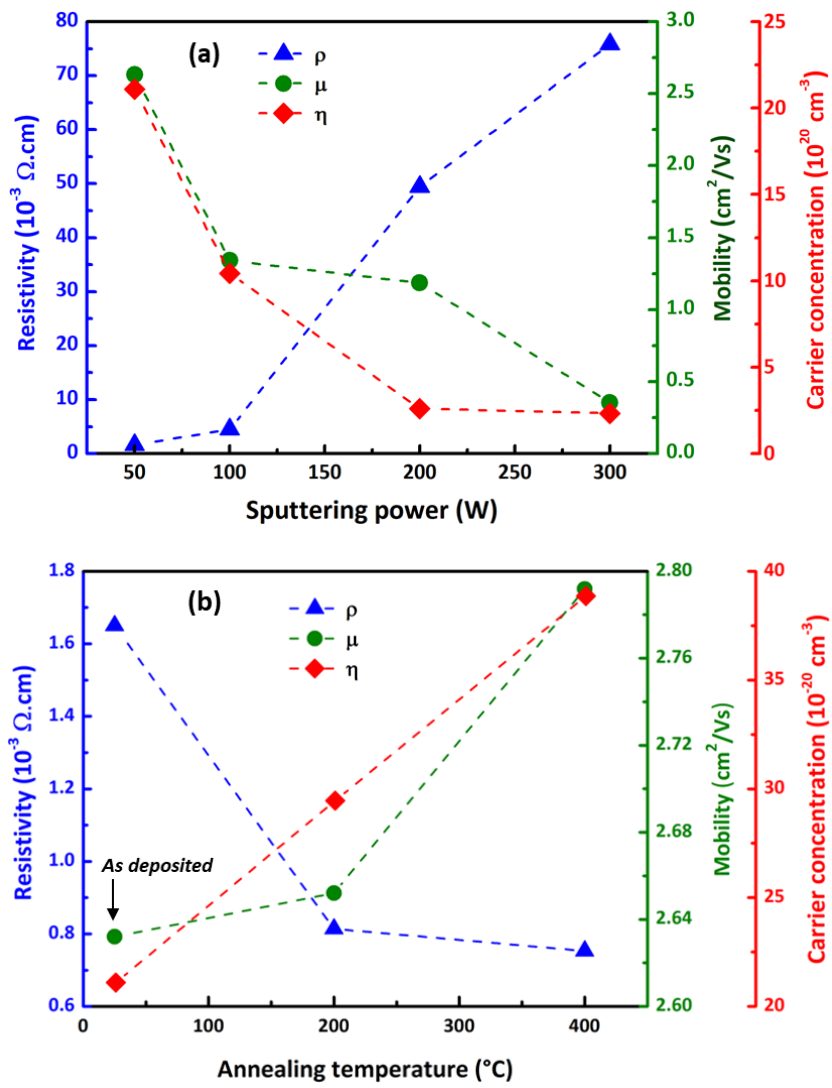


Fig. 8

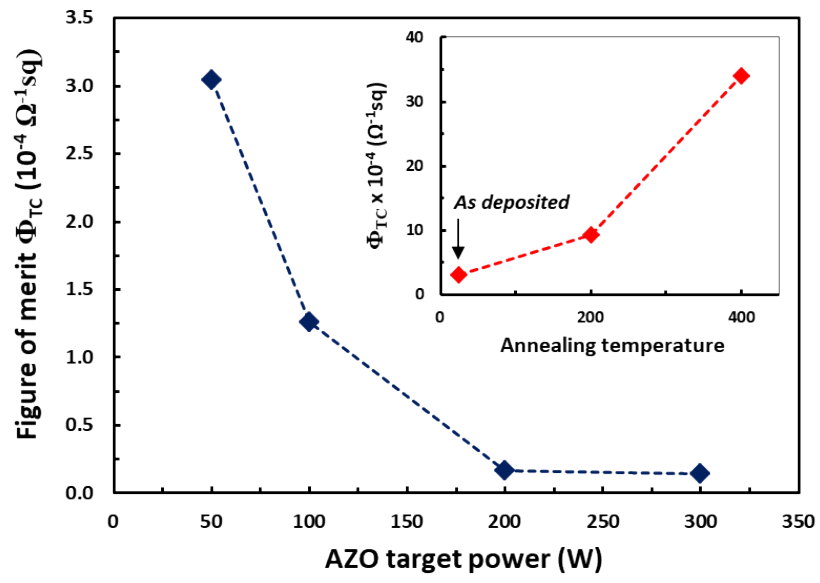


Fig. 9

Declaration of interests

☐ The authors declare that they have no known competing financial interests or personal relationships that could have appeared to influence the work reported in this paper.

☐ The authors declare the following financial interests/personal relationships which may be considered as potential competing interests:

--